# ABSTRACT

The role of singlet oxygen potentially mediating increased conformational flexibility of a disulfide was investigated. Density functional theory calculations indicate that the singlet oxygenation of 1,2-dimethyldisulfane produces a peroxy intermediate. This intermediate adopts a structure with a longer S–S bond distance and a more planar torsional angle  $\theta$  (C–S–S–C) compared to the non-oxygenated 1,2-dimethyldisulfane. The lengthened S–S bond enables a facile rotation about the torsional angle in the semicircle region  $0^{\circ} < \theta < 210^{\circ}$ , that is ~5 kcal/mol lower in energy than the disulfane. The peroxy intermediate bears no $\rightarrow \sigma s$ -s and no $\rightarrow \sigma * s$ -s interactions that stabilize the S–O bond but destabilize the S–S bond, which contrasts with stabilizing ns $\rightarrow \sigma * s$ -s hyperconjugative effects in the disulfane S–S bond. Subsequent departure of O<sub>2</sub> from the disulfane peroxy intermediate is reminiscent of peroxy intermediates which also expel O<sub>2</sub>, yet facilitate *cis-trans* isomerizations of stilbenes, hexadienes, cyanines, and carotenes. "Nonoxidative"  $^{1}$ O<sub>2</sub> interactions with a variety of bond types are currently underappreciated. We hope to raise awareness of how these interactions can help elucidate the origins of molecular twisting.

#### **INTRODUCTION**

The ability of photogenerated reactive oxygen intermediates to facilitate rotation of alkene and polyene bonds via peroxy intermediates has been the subject of a couple dozen studies (Figure 1) (1). In these studies, *trans-cis* isomerizations were shown to be triggered by visible light and the reversible addition of O<sub>2</sub>, with oxygen evolution and partial generation of the compound's

isomer via peroxy intermediates. We classify the formation of zwitterionic peroxy or diradical peroxy intermediates into three types: type I sensitized oxidation (oxygen radicals and radical ions) or type II sensitized oxidation ( ${}^{1}O_{2}$ ) reactions, or by substrate excitation in the presence of  $O_{2}$  (2-4).

52

48

49

50

51

53 [Figure 1 here]

54

55

56

57

58

59

60

61

62

63

64

65

66

67

68

69

70

This paper will focus mainly on peroxy intermediates from <sup>1</sup>O<sub>2</sub>-based reactions. A 2021 study described a <sup>1</sup>O<sub>2</sub>-based truncation reaction of heptamethine cyanine 1 to pentamethine cyanine 2; this reaction was thought to involve a zwitterionic peroxy intermediate with extended resonance of the positive charge formed from the attack of <sup>1</sup>O<sub>2</sub> on the C1' (Figure 2A) (5-7). DFT results implicated a zwitterionic peroxy intermediate, which readily twisted about a former C=C bond into a U-shaped structure on its way to two-carbon truncation to the pentamethine cyanine 2 (5). A 2000 study described a <sup>1</sup>O<sub>2</sub>-based isomerization of *trans*-4-propenylanisole 3 to *cis*-4, also thought to involve a zwitterionic peroxy intermediate (Figure 2B) (8). Furthermore, a phosphite trap suppressed the trans-3 to cis-4 isomerization, consistent with trapping of a peroxy intermediate. Other <sup>1</sup>O<sub>2</sub> reactions have led to *cis-trans* isomerizations of hexadienes (9,10), stilbenes (11), β-carotene and lycopene (12,13), also likely through peroxy intermediates. Relatedly, peroxy intermediates arise in various photooxidation and regular oxidation reactions. These intermediates include R<sub>2</sub>C<sup>+</sup>OO<sup>-</sup> carbonyl oxide, RN<sup>+</sup>OO<sup>-</sup> nitrosooxide, R<sub>2</sub>NN<sup>+</sup>(=O)OO<sup>-</sup> nitrooxide, R<sub>2</sub>Si<sup>+</sup>OO<sup>-</sup> silanone oxide, R<sub>2</sub>S<sup>+</sup>OO<sup>-</sup> persulfoxide, and R<sub>2</sub>Te<sup>+</sup>OO<sup>-</sup> pertelluroxide (14-25). Peroxy intermediates have been implicated in lowering the energy barrier for cistrans isomerization of alkene and polyene CC bonds (1). The motivation for our study is to explore

the possibility of this phenomenon occurring in disulfides. Here, we specifically address the effect of a non-oxidative <sup>1</sup>O<sub>2</sub> reaction on disulfide S–S torsional rotation.

73

71

72

# 74 [Figure 2 here]

75

76

77

78

79

80

81

82

83

84

85

86

87

88

89

90

91

92

93

A new twist on disulfide S–S bond rotation facilitated by <sup>1</sup>O<sub>2</sub>. To elucidate <sup>1</sup>O<sub>2</sub>'s influence on disulfide torsional rotation, we used DFT to analyze an intermediate from the reaction of 1,2dimethyldisulfane 5 with <sup>1</sup>O<sub>2</sub>, as a biomimetic model. Our hypothesis is that <sup>1</sup>O<sub>2</sub> will add to a disulfide, forming a zwitterionic peroxy intermediate, thereby inducing conformational relaxation of the S-S bond, with departure as <sup>1</sup>O<sub>2</sub> or <sup>3</sup>O<sub>2</sub> in a non-oxidative path. To test our hypothesis, we sought to use the above-mentioned DFT calculations to predict energy profiles, focusing on  $MeSS^{+}(-OO^{-})Me$ peroxythiosulfinate ester (peroxy-1,2-dimethyl- $1\lambda^3$ -disulfane, **6**). Hyperconjugative interactions in S-S serve to increase the energy of rotation in disulfane 5, accounting for the perpendicular arrangement as shown in Figure 3. We hypothesize that the effect will be less pronounced in 6 due to competitive hyperconjugative interactions in S-O. The importance of hyperconjugative interactions in 5 and 6 is found theoretically. Persulfoxide (R<sub>2</sub>S<sup>+</sup>OO<sup>-</sup>), S-hydroperoxysulfonium ylide [RS(-OOH)=CHR], and dioxathiirane (cyclic R<sub>2</sub>SO<sub>2</sub>) structures have been found to be minima in previous theoretical studies of the reaction of sulfides with  ${}^{1}O_{2}$  (26-28). DFT calculations with M06-2X can accurately reproduce the torsional barriers for simple disulfide S-S bonds, which are often 8-10 kcal/mol (29-32). However, reports of torsional barriers for peroxy disulfide S-S bonds are absent in the literature (33-35). Potential competitive charge-transfer interactions of <sup>1</sup>O<sub>2</sub> with disulfides (36) should not be overlooked, and will also be considered.

96 97

98

99

100

101

102

103

104

105

106

107

108

109

110

111

112

113

114

115

116

117

118

#### THEORETICAL SECTION

Density functional theoretical (DFT) calculations were carried out with Gaussian-16 (37) using recommended protocols (38,39). Structures were optimized with M06-2X/6-31+G(d,p) in the gas phase. Solvent effects were not anticipated to produce significant differences, and thus they were not calculated. The unrestricted M06-2X/6-31+G(d,p) energy of <sup>3</sup>O<sub>2</sub> was calculated to be -150.259899 Hartrees, in which the experimental singlet-triplet energy value of 22.5 kcal/mol was added to this calculated value of <sup>3</sup>O<sub>2</sub>. The stationary points on the potential energy surface (PES) were analyzed by harmonic vibrational frequency calculations. IRC calculations were carried out to verify the transition structures found from the M06-2X/6-31+G(d,p) calculations. The M06-2X/6-31+G(d,p) calculations are reasonably accurate for the predictions of dialkyldisulfane geometries and rotational energetics, based on comparisons with MP2 and CCSD(T) calculations (Table S1, Supporting Information). In our M06-2X calculations, basis set extension was examined with 6-311+G(d,p). We assessed dispersion corrections with B3LYP-D/6-31+G(d,p) and wB97XD/6-31+G(d,p) calculations. Coupled cluster calculations were carried out for comparison of M06-2X/6-31+G(d,p) results with single point CCSD(T)/6-31+G(d,p). DLPNO-CCSD(T)/6-31+G(d,p) calculations were also carried out using the ORCA program (version 4.0) (40). The conformational analysis in Figure 4 consists of M06-2X/6-31+G(d,p) optimized stationary points that where verified by vibrational analysis where minima had no imaginary frequencies and maxima had one imaginary frequency; the maxima were also analyzed by intrinsic reaction coordinate (IRC) calculations. The conformational analysis in Figure 4 consists of M06-2X/6-31+G(d,p) constrained optimizations, in which rotational energy profiles of 6 were followed in  $10^{\circ}$  increments with torsional constraints in torsional angle  $\theta$  (C1–S1–S2–C2) and the torsional angle  $\phi$  (S2–S1–O1–O2) (keyword: opt=ModRedundant). For the M06-2X calculations, an ultrafine grid with criteria for tight convergence were used (keywords: SCF=Tight int=grid=ultrafine). Molecular orbital interactions were examined with natural bonding orbital (NBO) calculations to quantify the attractive through-space interactions using NBO 7.0 (41,42) (keyword: E2PERT=0.1). The potential problem of spin contamination for **6** was examined using the T1 diagnostic of Lee and Taylor (43). Finally, DFT calculations are known to reproduce experimental disulfide and sulfur-oxygen intermediate structural features based on comparison to experimental structures (44-49). DFT methods such as M06-2X also perform well with sulfur-sulfur long pair interactions and in computing  $^{1}$ O<sub>2</sub> reactions leading to peroxy species (5,50).

### **RESULTS AND DISCUSSION**

Computed geometries of dimethyldisulfane 5 and peroxythiosulfinate ester 6 are discussed first. Conformational analyses of 2D and 3D computed energy plots are then described. An explanation of our approach to T1 diagnostics and NBO calculations will be followed by mechanistic considerations, and finally our thoughts on broader implications of the study.

Dimethyldisulfane 5 and peroxythiosulfinate ester 6. The calculated geometries of 5 and 6 (which arises from the reaction of 5 with  $^{1}\text{O}_{2}$ ) are shown in Figure 4. Figure 4 shows the calculated bond distance S1–S2, bond angle C1–S1–S2, and torsional angle  $\theta$  (C1–S1–S2–C2) for 5. In 5, the computed C1–S1 bond length is 1.820 Å, the S1–S2 bond length is 2.061 Å, the C1–S1–S2 bond angle is 101.9°, and  $\theta$  is 84.7°, which is similar to the reported microwave structure of diethyldisulfane: S1–S2 bond length of 2.027 Å, the C1–S1–S2 bond angle of 102.8°, and  $\theta$  of

84.5° (41). In **6**, the C1–S1 bond length is 1.802 Å, the S1–S2 bond length is 2.077 Å, the C2–S2 bond length is 1.824 Å, the S1–O1 bond length is 1.589 Å, the O1–O2 bond length is 1.436 Å, the C1–S1–S2 bond angle is 102.9°, and  $\theta$  is 41.5°. Comparing **6** to **5**, there is a bond distance increase of 0.016 Å (S1–S2), a bond angle increase of 1.0° (C1–S1–S2), and a torsional angle decrease of 43.2°  $\theta$  (C1–S1–S2–C2). How this leads to a more facile rotation about the C–S–S–C torsional angles in **5** and **6**, is explored next.

## [Figure 4 here]

Two-dimensional computed energy plot for rotation about the C–S–S–C torsional angles in 5 and 6. Figure 5 shows the computed rotational energy profiles about the torsional angle θ (C1–S1–S2–C2) for 5 and 6, both exhibiting a left-hand twisting motion. 5a and 5c are isoenergetic conformers with torsional angles θ gauche at 84.7° and 275.3°, respectively. The trans conformer 5b (180°, 7.5 kcal/mol) and cis conformer 5d (0°/360°, 10.5 kcal/mol) are transition states. For 6, the torsional angle θ is flatter; that is, in 6a there are two internal H-bonds at 41.5° (between O2 and flanking C–H), and a single internal H-bond 142.4° in 6c (between O2 and only the nearby C–H group). Note that we have colored the inner oxygen (O1) red and the outer oxygen (O2) magenta to make them easier to differentiate in Figure 4. Rotamer 6a is more stable than 6c by 0.3 kcal/mol. Transition states are found at 6b (102.3°, 2.4 kcal/mol) and 6d (322.0°, 9.2 kcal/mol). Comparing these results to computations using the basis set 6-31+G(3df,2p), the difference in precision was acceptable, varying 0.3-1.6 kcal/mol for 5a-d and 0-0.9 kcal/mol for 6a-d (Table S2, Supporting Information). The conformations for 5 appear to exhibit larger eclipsing energies with higher TS values compared to 6. Specifically, the extent of eclipsing interactions is lower by ~5 kcal/mol for

6 in the torsional angle  $\theta$  semi-circle range from 0 to ~210°, that is ~5 kcal/mol lower in energy than the disulfane. In this  $\theta$  semi-circle range, based on the Eyring equation the half-life for the rotation of S–S in 6 is only 3 ps, which is nearly 30,000-fold more rapid compared to the rotation of S–S in 6 (80,000 ps). Moreover, we find an energy decrease of 5.1 and 1.3 kcal/mol for the two maxima required to rotate 360° in 6 compared to 5 (Figure 4A and 4B). As it is important to ensure the quality of these computed results, we examined the 5.1 and 1.3 kcal/mol energy decrease values in the first and second maxima, both by extending the basis set and by testing for dispersion corrections.

We find that an extended basis set and accounting for dispersion corrections produced only minor differences. Comparing M06-2X/6-31+G(d,p) results with the extended basis set to 6-311+G(d,p) reduced TS energies by 0.3-2.0 kcal/mol for **5** and 1.7-3.9 kcal/mol for **6**. Comparing M06-2X/6-31+G(d,p) results with dispersion-corrected B3LYP-D/6-31+G(d,p) reduced TS energies by 0.3-1.7 kcal/mol for **5** and 2.7 kcal/mol for **6** ( $\theta = 102.3^{\circ}$ ) or increased it by 2.7 kcal/mol for **6** at ( $\theta = 322^{\circ}$ ). Comparing M06-2X/6-31+G(d,p) results with dispersion-corrected wB97XD/6-31+G(d,p) reduced TS energies by 0.1-1.6 kcal/mol for **5** and 2.0-2.5 kcal/mol for **6**. Thus, the errors appear to be constant for the basis set extension and dispersion corrections calculated. Additional conformational searches for **6** were desired, including about torsional angles  $\theta$  (C1–S1–S2–C2) and  $\varphi$  (S2–S1–O1–O2), as is described next.

184 [Figure 5 here]

Three-dimensional computed energy plot for rotations about the C-S-S-C and S-S-O-O torsional angles in **6**. To further investigate the conformational energetics of **6**, the S-S-O-O

torsional angles were analyzed in relation to maxima and minima about the C-S-S-C dihedral angle. Figure 6 shows the 360° rotation about these two torsional angles. As in the 2D plot (Figure 4), the inner oxygen (O1) of the 3D plot (Figure 6) is shown in red and the outer oxygen (O2) is shown in a magenta to help visually monitor the O1–O2 movement. Conformer 6a can convert to 6u via rotamers 6e, 6i, 6m, and 6q as seen in the magenta line trace about the torsional angle φ (S2–S1–O1–O2). Rotations about the torsional angle  $\theta$  are markedly lower that about the torsional angle φ, which is attributed to internal H-bond interactions of the outer oxygen atom (O2) with the methyl  $H_{\alpha}$ –C1 and  $H_{\beta}$ –C2. Conformers do not exist as minima when related by rotation about the torsion angle φ in an "out" position. Interestingly, most conformers exist as "open" zwitterionic peroxy intermediates in the computed energy plot, except for thio-dioxathiirane that is formed in 6i, 6j, 6k, and 6l upon rotation of the outer oxygen (O2) around the S2-O1, followed by ring closure. Note that these thio-dioxathiirane rotamers 6i, 6j, 6k, and 6l feature the lowest energies in the 3D plot (cf. Figure 6 with Figure S1), in which their formation also enhance rotation about θ compared to dimethyldisulfane 5 itself. The "open" zwitterionic peroxy intermediate 6a appears to be weakly bound with a long S–O bond. Therefore, we estimated the <sup>1</sup>O<sub>2</sub> dissociation in release of <sup>1</sup>O<sub>2</sub> from **6a** occurs on a flat portion of the reaction surface. Extension of the S–O bond length of **6a** in increments of 0.1 Å over 14 points, while monitoring the M06-2X/6-31+G(d,p) revealed the computed <sup>1</sup>O<sub>2</sub> dissociation barrier to be ~9 kcal/mol (endothermic by 6 kcal/mol). Extending the S-O bond lengths of thio-dioxathiirane 6i suggest a slightly larger, but still small <sup>1</sup>O<sub>2</sub> dissociation barrier of ~15 kcal/mol. This suggests the possibility that zwitterionic peroxy intermediates and thio-dioxathiiranes are weakly bound, potentially playing a role in subsequent oxygen departure. The transition state was neither sought nor traced by IRC. Nonetheless, the scan shows a low barrier for the dissociation of <sup>1</sup>O<sub>2</sub>, which would also provide for intersystem crossing

188

189

190

191

192

193

194

195

196

197

198

199

200

201

202

203

204

205

206

207

208

209

in the release as  ${}^{3}\text{O}_{2}$  (physical quenching). The scanned surface of **6** is similar to the previous Me<sub>2</sub>S<sup>+</sup>OO<sup>-</sup> persulfoxide study (26), which attributed the free energy surface barrier mainly to entropy; this was a determination validated by experimental results (51). The singlet-triplet energy gap of O<sub>2</sub> is 22.5 kcal/mol. This will enable an exothermic reaction (~16 kcal/mol) in the dissociation of  ${}^{3}\text{O}_{2}$  from **6**. However, this was not modeled further due to higher errors in this area of the reaction surface, as well as multiconfigurational computation challenges. Note that lower temperatures and nucleophilic solvents can potentially stabilize and retard the back reaction of **6** to **5** plus O<sub>2</sub>. Analogous to persulfoxides, peroxythiosulfinate ester **6** is a peroxy intermediate. Thus, it is potentially susceptible to spin contamination in M06-2X/6-31+G(d,p) calculations, which was evaluated next.

[Figure 6 here]

TI diagnostics and NBO calculations. The potential for spin contamination was examined for M06-2X/6-31+G(d,p) optimized structure 6 using T1 diagnostics. For 6, the T1 value was 0.018 using [CCSD(T,T1Diag,Full)/6-31+G(d,p)] and 0.019 using DLPNO-CCSD(T)/aug-cc-pVTZ/C. These results suggest an acceptable level of spin contamination that is not a significant issue for the reaction system, where T1 values that are greater than 0.02 for closed-shell systems or greater than 0.03 for open-shell systems point to unacceptable non-dynamical correlation or multiconfigurational character effects. Our DFT calculations support the idea that the outer oxygen is weakly bound to the disulfide, and participates in donor-acceptor interactions with the flanking methyl groups.

Results of NBO calculations show attractive through-space interactions of the outer oxygen atom (O2) lone pair electrons (lp) with the  $\sigma^*$  orbitals of  $H_{\alpha}$ –C1 and  $H_{\beta}$ –C2 (Figure 7). These interactions were quantified to give 4.1 and 3.5 kcal/mol stabilization, respectively. This net in energetics of 7.6 kcal/mol indicates the favorability for the "in" position, in which the O1–O2 bond bisects the C1–S1–S2 bond angle. Notice in 6 that O1–O2 bisecting the C1–S1–S2 bond angle, induces a distorted tetrahedral geometry, where the C1–H···O2 bond distance is 2.224 Å and the C2–H···O2 bond distance is 2.313 Å. Previous reports (26-28) also show that the persulfoxide also favors an "in" position with its O–O bond bisecting two alkyl groups.

### [Figure 7 here]

Mechanistic considerations. Peroxy intermediate 6 is formed upon reaction of  ${}^{1}O_{2}$  with disulfane 5. Based on DFT studies, we find that (i) this intermediate rotates about S–S, concurrent with an activation barrier reduction. Though this decrease in energy that we propose is significant, it is smaller in magnitude compared to that found in C=C rotation in alkenes and polyenes alluded to in the Introduction. (ii) The 2D and 3D plots show that a stable conformer of 6 is with attached oxygen positioned "in," where rotation about θ is more facile than about φ. This bias towards "in" is understood to be a result of C–H···O interactions of the outer oxygen atom with the flanking methyl groups. (iii) Dispersion corrections led to similar torsional rotation energies for 5 and 6. Thus, the M06-2X/6-31+G(d,p) results are reasonable for the predicted energy of rotation about a disulfide S–S. (iv) Stepwise extension of the S–O bond length of 6 leads to a predicted  ${}^{1}O_{2}$  dissociation of ~9 kcal/mol (endothermic by ~6 kcal/mol). Our computations predict that energies lie on the side of 6 instead of the reactants 5 and  ${}^{1}O_{2}$ , which is consistent with persulfoxides that are sufficiently long lived to be trapped bimolecularly and play a role in

converting  ${}^{1}O_{2}$  to  ${}^{3}O_{2}$  (52-54). Unlike some acene endoperoxides (55-62),  ${}^{1}O_{2}$  "on-off" is likely accompanied by substantial physical quenching to  ${}^{3}O_{2}$  in regeneration of the disulfane. Indeed, charge-transfer quenching of  ${}^{1}O_{2}$  with disulfides can involve an exciplex MeSS(··· ${}^{1}O_{2}$ )Me that physically quenches  ${}^{1}O_{2}$  to  ${}^{3}O_{2}$  due to sulfur's low-lying *d*-orbitals (36). While the exciplex may be in equilibrium with the covalently bound MeSS<sup>+</sup>( ${}^{+}OO^{-}$ )Me 6 species, it is the latter that is invoked in facilitating the S–S rotation.

Origin and broader implications. Disulfane 5 bears two lone-pair (lp) electron interactions in  $n_{S(axial)} \rightarrow \sigma^*_{S-S}$  and  $n_{S(equatorial)} \rightarrow \sigma^*_{S-S}$  for a pronounced negative hyperconjugation in reducing repulsion among lone pairs. This is an anomeric effect (63), favoring a skew conformation in 5 ( $\theta$ = 84.7°). One pair of sulfur electrons from 5 can donate into the empty  $\pi_g$  orbital of  ${}^{1}O_2$  to account for the formation of peroxythiosulfinate ester 6. Comparing 6 with 5, there are several important differences: 6 shows an elimination of one of the hyperconjugative interactions, with addition of stabilizing no+ $\sigma_{S-S}$  and modestly destabilizing no- $\sigma_{S-S}$ + $\sigma_{S-S}$  and no- $\sigma_{S-S}$  interactions. Together, these aspects account for an increase and weakening of the S-S bond length in 6, in which the methyl (Me), methylsulfane (–SMe), and O<sub>2</sub> groups are attached at a sulfonium ion-like S-atom. Implications for singlet oxygen's role as a non-oxidative facilitator of S-S bond rotation in other systems, including relaxation of protein disulfide rigidity, are quite plausible. Just as fascinating to us is the possibility that torsional flexibility could offer anti-photooxidant activity by converting excited-state <sup>1</sup>O<sub>2</sub> to ground-state <sup>3</sup>O<sub>2</sub> by means of a conformational energy-releasing process. Intriguingly, this process has been seen in azobenzene (70). Finally, it should be noted that other reagents, such as protons, should be explored as candidates that might also facilitate rotations of S–S bonds.

257

258

259

260

261

262

263

264

265

266

267

268

269

270

271

272

273

274

275

276

277

### **CONCLUSION**

Our computed study of a peroxy intermediate **6** arising in a  $^{1}O_{2}$  reaction with dimethyldisulfane **5** was directly inspired by reports of peroxy intermediates from  $^{1}O_{2}$  facilitating *trans-cis* isomerizations of alkene and polyene bonds (1). The current work adds crucial insight to the basis of the lower torsional barrier of the peroxy intermediate **6** relative to disulfane **5**. Further studies could include peroxythiosulfinate ester decomposition to  $^{1}O_{2}$  or  $^{3}O_{2}$  to assess the non-oxidative path relative to S–S bond cleavage, oxidation, and biological cross-linking reactions (64-69). Further studies will also explore the possibility that torsional flexibility correlates to antioxidant activity in converting excited-state  $^{1}O_{2}$  to  $^{3}O_{2}$  through a physical quenching process. Also, future work could examine disulfide peroxy intermediates formed by a type I process, featuring oxygen radicals and radical ions (as opposed to exclusive type II  $^{1}O_{2}$  mediation), since a type I process is feasible for alkenes and polyenes seen in Figure 1 (1).

### **Supporting Information**

Supporting Information is available, which includes descriptions of energies and geometries of stationary points.

#### **ORCID**

Oliver Turque 0000-0001-8987-8546

303 Ryan M. O'Connor 0000-0003-3623-7387 304 Alexander Greer: 0000-0003-4444-9099 305 306 Acknowledgments 307 We thank the National Science Foundation (CHE-2154133) for funding. This work used Expanse 308 in the Extreme Science and Engineering Discovery Environment (XSEDE) cluster at the San 309 Diego Supercomputer Center, which is supported by the NSF (ACI-1548562) through allocation 310 CHE-210052. We thank Leda Lee for the graphic arts work. 311 312 313 References 314 (1) Turque, O., A. Greer and O. R. Wauchope (2020) Synthetic feasibility of oxygen-driven 315 photoisomerizations of alkenes and polyenes. Org. Biomol. Chem. 18, 9181-9190. 316 (2) Baptista, M. S., J. Cadet, P. Di Mascio, A. A. Ghogare, A. Greer, M. R. Hamblin, C. Lorente; 317 S. C. Nunez, M. S. Ribeiro, A. H. Thomas, M. Vignoni and T. M. Yoshimura (2017) Type II 318 and type II photosensitized oxidation reactions: Guidelines and mechanistic pathways. 319 *Photochem. Photobiol.* **93**, 912-919. 320 (3) Baptista, M. S., J. Cadet, A. Greer, A. H. Thomas (2021) Photosensitization reactions of 321 biomolecules: Definition, targets, and mechanisms. *Photochem. Photobiol.* **97**, 1456-1483. 322 (4) Di Mascio, P., G. R. Martinez, S. Miyamoto, G. E. Ronsein, M. H. G. Medeiros and J. Cadet 323 (2019) Singlet molecular oxygen reactions with nucleic acids, lipids, and proteins. Chem. Rev.

324

**119**, 2043-2086

- 325 (5) Matikonda, S. S., D. A. Helmerich, M. Meub, G. Beliu, P. Kollmannsberger, A. Greer, M.
- 326 Sauer and M. J. Schnermann (2021) Defining the basis of cyanine phototruncation enables a
- new approach to single-molecule localization microscopy. ACS Cent. Sci. 7, 1144-1155.
- 328 (6) Fukushima, H., S. S. Matikonda, S. M. Usama, A. Furusawa, T. Kato, L. Stackova, P. Klan,
- H. Kobayashi and M. J. Schnermann (2022) Cyanine phototruncation enables spatiotemporal
- 330 cell labeling. J. Am. Chem. Soc. **144**, 11075-11080.
- 331 (7) Helmerich, D. A., G. Beliu, G., S. S. Matikonda, M. J. Schnermann and M. Sauer (2021)
- Photoblueing of organic dyes can cause artifacts in super-resolution microscopy. *Nat.*
- 333 *Methods* **18**, 253–257.
- 334 (8) Greer, A., G. Vassilikogiannakis, K.-C. Lee, T. S. Koffas, K. Nahm and C. S. Foote (2000)
- Reaction of singlet oxygen with *trans*-4-propenylanisole. Formation of [2 + 2] products with
- 336 added acid. J. Org. Chem. 65, 6876-6878.
- 337 (9) O'Shea, K. E. and C. S. Foote (1988) Chemistry of singlet oxygen. 51. Zwitterionic
- intermediates from 2,4-hexadienes. J. Am. Chem. Soc. 110, 7167-7170.
- 339 (10) Leach, A. G., K. N. Houk and C. S. Foote (2008) Theoretical prediction of a perepoxide
- intermediate for the reaction of singlet oxygen with *trans*-cyclooctene contrasts with the two-
- step no-intermediate ene reaction for acyclic alkenes. *J. Org. Chem.* **73**, 8511-8519.
- 342 (11) Saltiel, J. and R. F. Klima (2006) α-Methylstilbene and the duality of mechanism in the
- quenching of stilbene triplets by molecular oxygen. *Photochem. Photobiol.*, 2006, 82, 38-42.
- 344 (12) Heymann, T., P. Heinz and M. A. Glomb (2015) Lycopene inhibits the isomerization of β-
- carotene during quenching of singlet oxygen and free radicals J. Agric. Food Chem., 63, 3279-
- 346 3287.

- 347 (13) Heymann, T., L. M. Schmitz, J. Lange and M. A. Glomb (2020) Influence of β-carotene and
- 348 lycopene on oxidation of ethyl linoleate in one- and disperse-phased model systems *J. Agric*.
- 349 Food Chem., **68**, 2747-2756.
- 350 (14) Sander, W. (2014) Carbonyl oxides—Rising stars in tropospheric chemistry. *Angew. Chem.*
- 351 *Int. Ed.* **53**, 362-364.
- 352 (15) Kuwata, K. T. (2014) Quantum chemical studies of carbonyl oxide chemistry in combustion
- and in the lower atmosphere. In *Chemistry of Peroxides, Vol. 3*, pp. 585-632. John Wiley &
- 354 Sons, Ltd.
- 355 (16) Chainikova, E. M., S. L. Khursan and R. L. Safiullin (2014) The chemistry of nitroso oxides.
- In Chemistry of Peroxides Vol 3, pp. 357-420. John Wiley & Sons, Ltd.
- 357 (17) Ghogare, A. A., C. J. Debaz, M. S. Oliveira, I. Abramova, P. P. Mohapatra, K. Kwon, E. M.
- Greer, F. M. Prado, H. P. Valerio, P. Di Mascio and A. Greer (2017) Experimental and DFT
- computational insight into nitrosamine photochemistry—Oxygen matters. J. Phys. Chem.
- 360 A. **121**, 5954-5966.
- 361 (18) Oliveira, M. S., A. A. Ghogare, I. Abramova, E. M. Greerm, F. M. Prado, P. Di Mascio and
- A. Greer (2015) Mechanism of photochemical O-atom exchange in nitrosamines with
- 363 molecular oxygen. J. Org. Chem. **80**, 6119-6127.
- 364 (19) Sander, W., M. Trommer and A. Patyk (1998) Oxidation of silenes and silylenes: Matrix
- isolation of unusual silicon species. In Organosilicon Chemistry III: From Molecules to
- 366 *Materials* (Edited by N. Auner and J. Weis) pp. 86-94. Muenchner Silicontage, 3<sup>rd</sup>, Munich.
- 367 (20) Monsour, C. G., C. M. Decosto, B. J. Tafolla-Aguirre, L. A. Morales and M. Selke (2021)
- 368 Singlet oxygen generation, quenching and reactivity with metal thiolates. *Photochem*.
- 369 *Photobiol.* **97**, 1219-1240.

- 370 (21) Zhang, D., Y. Bin, L. Tallorin, F. Tse, B. Hernandez, E. V. Mathias, T. Stewart, R. Bau and
- M. Selke (2013) Sequential photooxidation of a Pt(II) (diimine)cysteamine complex:
- Intermolecular oxygen atom transfer versus sulfinate formation. *Inorg. Chem.* **52**, 1676-1678.
- 373 (22) Sawwan, N. and A. Greer (2007) Rather exotic types of cyclic peroxides: Heteroatom
- 374 dioxiranes. Chem. Rev. 107, 3247-3285.
- 375 (23) Bonesi, S. M., M. Fagnoni and A. Albini (2004) Hammett correlations in the photosensitized
- oxidation of 4-substituted thioanisoles. *J. Org. Chem.* **69**, 928-935.
- 377 (24) Clennan, E. L. (2001) Persulfoxide: Key intermediate in reactions of singlet oxygen with
- 378 sulfides. Acc. Chem. Res. 34, 875–884.
- 379 (25) Clark, J. L., J. E. Hill, I. D. Rettig, J. J. Beres, R. Ziniuk, T. Y. Ohulchanskyy, T. M.
- McCormick and M. R. Detty (2019) Importance of singlet oxygen in photocatalytic reactions
- of 2-aryl-1,2,3,4-tetrahydroisoquinolines using chalcogenorosamine photocatalysts.
- 382 *Organometallics* **38**, 2431-2442.
- 383 (26) Jensen, F., A. Greer and E. L. Clennan (1998) Reaction of organic sulfides with singlet
- 384 oxygen. A revised mechanism. *J. Am. Chem. Soc.* **120**, 4439-4449.
- 385 (27) McKee, M. J. (1998) A theoretical study of unimolecular reactions of dimethyl persulfoxide.
- 386 J. Am. Chem. Soc. 120, 3963-3969.
- 387 (28) Greer, A., M.-F. Chen, F. Jensen and E. L. Clennan (1997) Experimental and ab initio
- 388 computational Evidence for new peroxidic intermediates (iminopersulfinic acids).
- Substituent effects in the photooxidations of sulfenic acid derivatives. J. Am. Chem. Soc. 119,
- 390 4380-4387.

- 391 (29) Zhang, J., H. Ye, Y. Jin, Q. Gou, M. Biczysko and G. Feng (2019) Conformational equilibria
- and molecular structures of model sulfur-sulfur bridge systems: Diisopropyl disulfide. J.
- 393 *Phys. Chem. A* **123**, 10714-10720.
- 394 (30) Zhang, J., X. Li, Q. Gou and G. Feng (2018) Disulfide bond in diethyl disulfide: A rotational
- 395 spectroscopic study. *J. Phys. Chem. A* **122**, 5597-5601.
- 396 (31) Priefer, R., Y. J. Lee, F. Barrios, J. H. Wosnick, A.-M. Lebuis, P. G. Farrell and D. N. Harpp
- 397 (2002) Dicubyl disulfide. *J. Am. Chem. Soc.* **124**, 5626-5627.
- 398 (32) Fraser, R. R., G. Boussard, J. K. Saunders, J. B. Lambert and C. E. Mixan (1971) Barriers to
- rotation about the sulfur-sulfur bond in acyclic disulfides. J. Am. Chem. Soc. 93, 3822-3823.
- 400 (33) Lu, W., I. H. Tsai, Y. Sun, W. Zhou and J. Liu (2017). Elucidating potential energy surfaces
- for singlet O<sub>2</sub> reactions with protonated, deprotonated, and di-dedeprotonated cystine using a
- 402 combination of approximately spin-projected density functional theory and guided-ion-beam
- 403 mass spectrometry. *J. Phys. Chem. B* **121**, 7844-7854.
- 404 (34) Lacombe, S., M. Loudet, A. Dargelos and E. Robert-Banchereau (1998) Oxysulfur
- 405 compounds derived from dimethyl disulfide: An ab initio study. J. Org. Chem. 63, 2281-2291.
- 406 (35) Lacombe, S., H. Cardy, M. Simon, A. Khoukh, J. Soumillion and M. Ayadim (2002)
- Oxidation of sulfides and disulfides under electron transfer or singlet oxygen
- photosnsitization using soluble or grafted sensitizers. *Photochem. Photobiol. Sci.* 1, 347-354.
- 409 (36) Clennan, E. L., D. Wang, C. Clifton and M.-F. Chen (1997) Geometry-dependent quenching
- of singlet oxygen by dialkyl disulfides. J. Am. Chem. Soc. 119, 9081-9082.
- 411 (37) Frisch, M. J., G. W. Trucks, H. B. Schlegel, G. E. Scuseria, M. A. Robb, J. R. Cheeseman, G.
- Scalmani, V. Barone, G. A. Petersson, H. Nakatsuji, X. Li, M. Caricato, A. V. Marenich, J.
- Bloino, B. G. Janesko, R. Gomperts, B. Mennucci, H. P. Hratchian, J. V. Ortiz, A. F.

- Izmaylov, J. L. Sonnenberg, D. Williams-Young, F. Ding, F. Lipparini, F. Egidi, J. Goings,
- B. Peng, A. Petrone, T. Henderson, D. Ranasinghe, V. G. Zakrzewski, J. Gao, N. Rega, G.
- Zheng, W. Liang, M. Hada, M. Ehara, K. Toyota, R. Fukuda, J. Hasegawa, M. Ishida, T.
- Nakajima, Y. Honda, O. Kitao, H. Nakai, T. Vreven, K. Throssell, J. A. Montgomery, Jr., J.
- E. Peralta, F. Ogliaro, M. J. Bearpark, J. J. Heyd, E. N. Brothers, K. N. Kudin, V. N.
- Staroverov, T. A. Keith, R. Kobayashi, J. Normand, K. Raghavachari, A. P. Rendell, J. C.
- Burant, S. S. Iyengar, J. Tomasi, M. Cossi, J. M. Millam, M. Klene, C. Adamo, R. Cammi, J.
- W. Ochterski, R. L. Martin, K. Morokuma, O. Farkas, J. B. Foresman and D. J. Fox, *Gaussian*
- 422 *16*, Revision C.01; Gaussian, Inc.: Wallingford, CT, 2016.
- 423 (38) Jensen, F. (2021) Computational chemistry: The exciting opportunities and the boring details.
- 424 *Isr. J. Chem.* **62**, e202100027.
- 425 (39) Jensen, F. (2017) How large is the elephant in the density functional theory room? *J. Phys.*
- 426 *Chem. A* **121**, 6104-6107.
- 427 (40) Neese, F. (2017) Software update: The ORCA program system, version 4.0, *Wiley Interdiscip*.
- 428 Rev.: Comput. Mol. Sci. 8, e1327.
- 429 (41) Glendening, E. D., J, K. Badenhoop, A. E. Reed, J. E. Carpenter, J. A. Bohmann, C. M.
- Morales, P. Karafiloglou, C. R. Landis, and F. Weinhold (2018) NBO 7.0. Theoretical
- Chemistry Institute, University of Wisconsin, Madison.
- 432 (42) Liakos, D. G., M. Sparta, M. K. Kesharwani, J. M. L. Martin and F. Neese (2015) Exploring
- the accuracy limits of local pair natural orbital coupled-cluster theory. J. Chem. Theory
- 434 *Comput.* **11**, 1525-1539.
- 435 (43) Lee, T. J. and P. R. Taylor (1989) A diagnostic for determining the quality of single-reference
- electron correlation methods. *Int. J. Quantum Chem., Quantum Chem. Symp.* **36**, 199-207.

- 437 (44) Sąsiadek, W., I. Bryndal, T. Lis, M. Wandas and J. Hanuza (2022) Synthesis and
- physicochemical properties of the methyl-nitro-pyridine-disulfide: X-ray, NMR, electron
- absorption and emission, IR and Raman studies and quantum chemical calculations. J. Mol.
- 440 Struct. **1257**, 132535.
- 441 (45) Durant, A. G., E. A. Nicol, B. M. McInnes and A. L. Schwan (2022) A DFT examination of
- the role of proximal boron functionalities in the S-alkylation of sulfenic acid anions. Org.
- 443 Biomol. Chem. **20**, 649-657.
- 444 (46) Schwan, A. L., M. M. Michalski, J. P. Findlay (2019) Origins and applications of
- stereoselective sulfenate anion alkylation reactions. *Phosphorus, Sulfur Silicon Relat.*
- 446 Elem. **194**, 692-697.
- 447 (47) Schwan, A. L. (2019) A computational determination of the origins of diastereoselective
- alkylations of a cysteinesulfenate anion. Eur. J. Org. Chem. 519-526.
- 449 (48) Zhang, Z., W. Li, J. Liu, X. Chen and Y. Bu (2012) DFT studies on the mechanism of the
- conversion of thiols into disulfides and dihydrogen catalyzed by CpMn(CO)<sub>3</sub> complex. J.
- 451 *Organmet. Chem.* **706**/**707**, 89-98.
- 452 (49) Hudaky, I., Z. Gaspari, O. Carugo, M. Cemazar, S. Pongor and A. Perczel (2004) Vicinal
- disulfide bridge conformers by experimental methods and by *ab initio* and DFT molecular
- 454 computations. *Proteins* **55**, 152-168.
- 455 (50) Hudson, B. M., E. Nguyen and D. J. Tantillo (2016) The influence of intramolecular sulfur-
- lone pair interactions on small-molecule drug design and receptor binding. Org. Biomol. 14,
- 457 3975-3980.

- 458 (51) Clennan, E. L., K. A. Oolman, K. Yang and D. X. Wang (1991) Effect of temperature on
- sulfide photooxidations. Evidence for a reversibly formed exciplex. J. Org. Chem. 56, 4286-
- 460 4289.
- 461 (52) Liang, J.-J., C.-L. Gu, M. L. Kacher and C. S. Foote (1983) Chemistry of singlet oxygen 45.
- Mechanism of the photooxidation of sulfides. J. Am. Chem. Soc. 105, 4717-4721.
- 463 (53) Clennan, E. L. (1995) Sulfide photooxidation. A question in mechanism. In: Advances in
- Oxygenated Processes Vol. 4 (Edited by A. L. Baumstark) JAI Press: Greenwich, CT, pp 49-
- 465 80.
- 466 (54) Clennan, E. L. and D. Aebisher (2002) The first example of a singlet oxygen induced double
- bond migration during sulfide photooxidation. Experimental evidence for sulfone formation
- via a hydroperoxy sulfonium ylide. *J. Org. Chem.* **67**, 1036-1037.
- 469 (55) Clennan, E. L. (2023) Aromatic endoperoxides. Photochem. Photobiol.
- 470 https://doi.org/10.1111/php.13674.
- 471 (56) Bedi, A., A. Manor Armon and O. Gidron (2020) Effect of twisting on the capture and release
- of singlet oxygen by tethered twisted acenes. *Org. Lett.* **22**, 7809-7813.
- 473 (57) Fudickar, W. and T. Linker (2019) Theoretical insights into the effect of solvents on the [4 +
- 2] cycloaddition of singlet oxygen to substituted anthracenes: A change from a stepwise
- process to a concerted process. J. Phys. Org. Chem. 32, e3951.
- 476 (58) Ucar, E., D. Xi, O. Seven, C. Kaya, X. Peng, W. Sun and E. U. Akkaya (2019) "Off-on"
- switching of intracellular singlet oxygen release under biocompatible conditions. *Chem.*
- 478 *Commun.* **55**, 13808-13811.
- 479 (59) Thomas III, S.W., E. Altinok, and J. Zhang (2016) Cycloadditions of singlet oxygen for
- responsive fluorescent polymers. *Synlett.* **27**, 355-368.

- 481 (60) Fudickar, W. and T. Linker (2014) In Patai's Chemistry of Functional Groups, The Chemistry
- 482 of Peroxides, Vol. 3. pp. 21-86. John Wiley & Sons Ltd.
- 483 (61) Fudickar, W. and T. Linker (2008) Remote substituent effects on the photooxygenation of
- 9,10-diarylanthracenes: Strong evidence for polar intermediates. *Chem. Commun.* 1771-1773.
- 485 (62) Chien, S.-H., M.-F. Chen, K.-C. Lau and W.-K. Li (2005) Theoretical study of the Diels-
- Alder reactions between singlet ( $^{1}\Delta_{g}$ ) oxygen and acenes. J. Phys. Chem. A 109, 7509-7518.
- 487 (63) Alabugin, I. V., L. Kuhn, N. V. Krivoshchapov, P. Mehaffya and M. G. Medvedev (2021)
- Anomeric effect, hyperconjugation and electrostatics: Lessons from complexity in a classic
- stereoelectronic phenomenon. *Chem. Soc. Rev.* **50**, 10212-10252.
- 490 (64) Jiang, S., L. Carroll, L. M. Rasmussen and M. J. Davies (2021) Oxidation of protein disulfide
- bonds by singlet oxygen gives rise to glutathionylated proteins. *Redox Biol.* **38**, 101822.
- 492 (65) Shi, W.-J., D. K. P. Ng, S. Zhao and P.-C. Lo (2019) A phthalocyanine-based glutathione-
- activated photosensitizer with a ferrocenyl boron dipyrromethene dark quencher for
- photodynamic therapy. *ChemPhotoChem* **3**, 1004-1013.
- 495 (66) Chow, S. Y. S., S. Zhao, P.-C. Lo and D. K. P. Ng (2017) A cell-selective glutathione-
- responsive tris(phthalocyanine) as a smart photosensitiser for targeted photodynamic therapy.
- 497 Dalton Trans. 46, 11223-11229.
- 498 (67) Karimi, M., M. T. Ignasiak, B. Chan, A. K. Croft, L. Radom, C. H. Schiesser, D. I. Pattison
- and M. J. Davies (2016) Reactivity of disulfide bonds are markedly affected by structure and
- environment: implications for protein modification and stability. *Sci. Rep.* **6**, 38572.
- 501 (68) Chohan, B. S., S. C. Shoner, J. A. Kovacs and M. J. Maroney (2004) Ligand oxidations in
- high-spin nickel thiolate complexes and zinc analogues. *Inorg. Chem.* **43**, 7726-7734.

503	(69) Devasagayam, T. P. A., P. Di Mascio, S. Kaiser and H. Sies (1991) Singlet oxygen induced
504	single-strand breaks in plasmid pBR322 DNA: The enhancing effect of thiols. Biochimica et
505	Biophysica Acta 1088, 409-412.
506	(70) Kuntze, K., J. Isokuortti, A. Siiskonen, N. Durandin, T. Laaksonen, and A. Priimagi (2021)
507	Azobenzene photoswitching with near-infrared light mediated by molecular oxygen. J. Phys.
508	Chem. B. 125, 12568-12573.
509	
510	
511	FIGURE CAPTIONS
512	Figure 1. Mechanistic pathways for O <sub>2</sub> -dependent photoisomerization. Ground-state sensitizer
513	(sens <sub>0</sub> ) is photoexcited to reach its triplet state, where reactions can proceed by oxygen radicals
514	and radical ions (type I) or singlet oxygen ( <sup>1</sup> O <sub>2</sub> , type II), or by direct excitation of the substrate in
515	the presence of O2. Alkene and polyene compounds can form oxidized products, but also traces of
516	isomerized products presumably by zwitterionic or diradical peroxy intermediates.
517	
518	Figure 2. Zwitterionic peroxy intermediates presumably responsible for rotation and trans-cis
519	isomerization reactions in paths A and B.
520	
521	Figure 3. Hyperconjugative interactions that leads to delocalizations in dimethyldisulfane 5 and
522	peroxythiosulfinate ester 6.
523	
524	<b>Figure 4.</b> M06-2X/6-31+G(d,p) computed dimethyldisulfane <b>5</b> and peroxythiosulfinate ester <b>6</b> .

Figure 5. M06-2X/6-31+G(d,p) computed rotational energy profiles of dimethyldisulfane 5 (left) and peroxythiosulfinate ester 6 (right). Conformers C-S-S-C are related by rotation about the torsion angle  $\theta$  in a counterclockwise movement about the C1–S1 bond relative to the S2–C2 bond. In 6, the inner oxygen atom is red and the outer oxygen atom is a magenta color. **Figure 6.** Three-dimensional computed energy plot for the 360° rotation about the dihedral angles  $\theta$  (C1–S1–S2–C2) and  $\varphi$  (S2–S1–O1–O2). The torsional angles  $\theta$  (C1–S1–S2–C2) and  $\varphi$  (S2–S1– O1–O2) were followed in  $10^{\circ}$  constrained increments each for the  $360^{\circ}$  rotation in a  $36 \times 36$  grid. Conformers of C1-S1-S2-C2 are related by rotation about the torsion angle  $\theta$  in a counterclockwise movement about the C1-S1 bond relative to the S2-C2 bond. Conformers of S2-S1-O1-O2 are related by rotation about the torsion angle  $\varphi$  in a counterclockwise movement about the S1–S2 bond relative to the O1–O2 bond. Values shown are  $\theta$  and  $\varphi$  (°) and  $\Delta E$  (kcal/mol). Figure 7. A Natural Bond Orbital (NBO) analysis of the outer oxygen atom lone pair electrons with the  $\sigma^*$  antibonding orbitals of H–C groups in peroxythiosulfinate ester 6. 

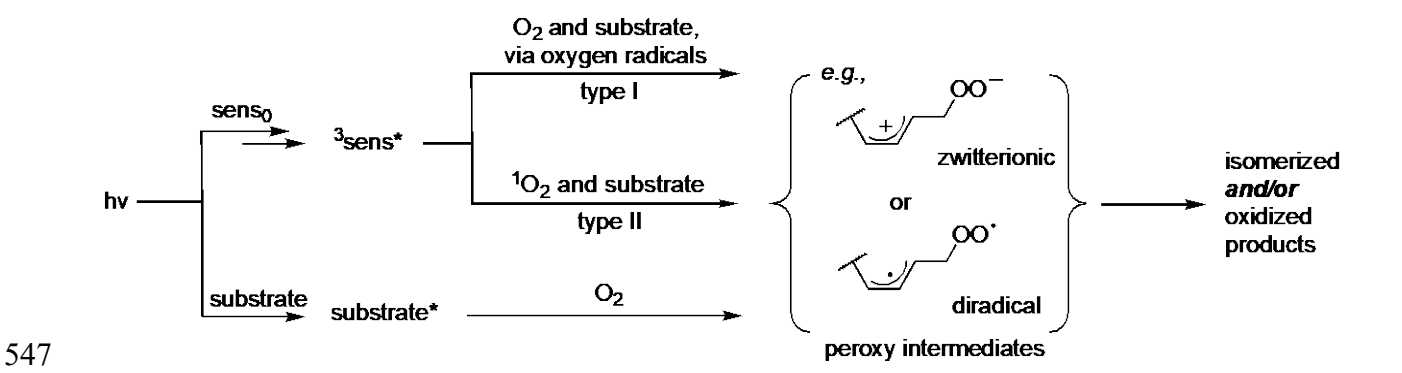


**Figure 1.** Mechanistic pathways for O<sub>2</sub>-dependent photoisomerization. Ground-state sensitizer (sens<sub>0</sub>) is photoexcited to reach its triplet state, where reactions can proceed by oxygen radicals and radical ions (type I) or singlet oxygen (<sup>1</sup>O<sub>2</sub>, type II), or by direct excitation of the substrate in the presence of O<sub>2</sub>. Alkene and polyene compounds can form oxidized products, but also traces of isomerized products presumably by zwitterionic or diradical peroxy intermediates.

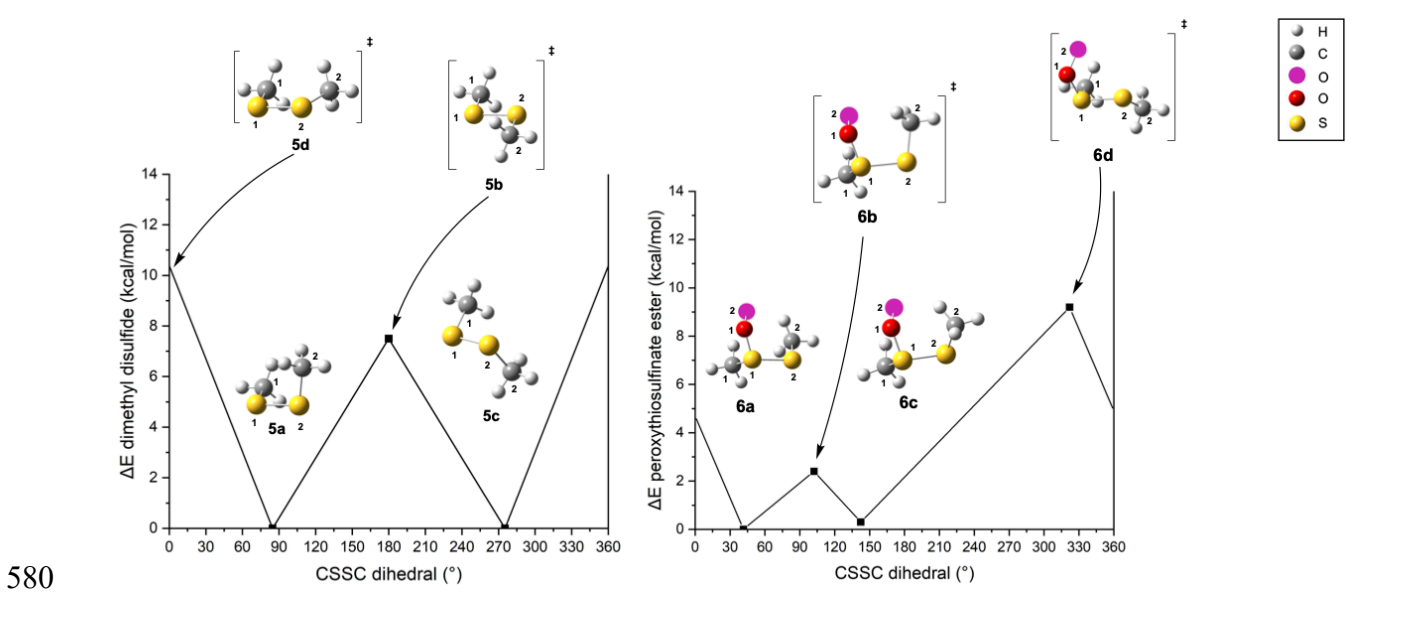
**Figure 2.** Zwitterionic peroxy intermediates presumably responsible for rotation and *trans-cis* isomerization reactions in paths A and B.

Figure 3. Hyperconjugative interactions that leads to delocalizations in dimethyldisulfane 5 and

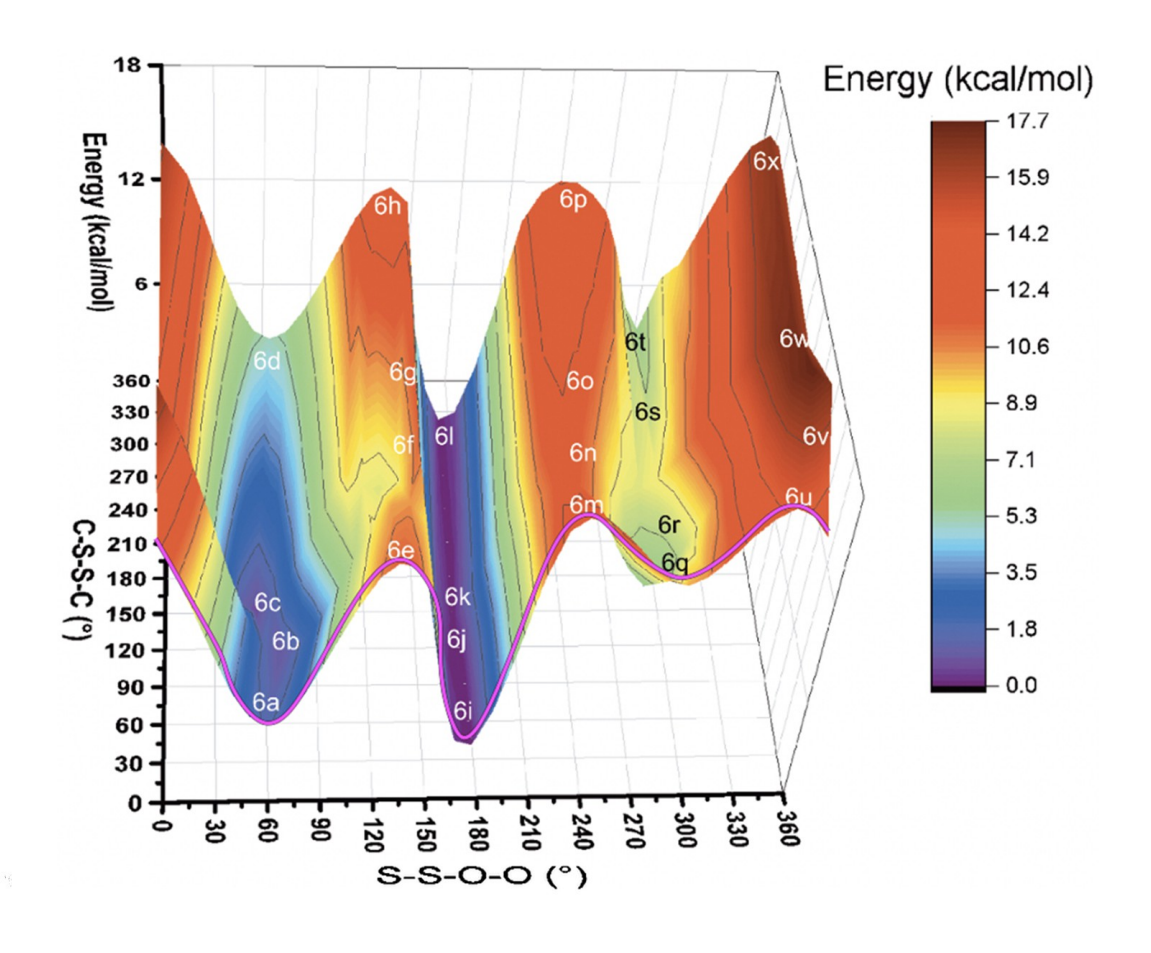
peroxythiosulfinate ester **6**.

Figure 4. M06-2X/6-31+G(d,p) computed dimethyldisulfane 5 and peroxythiosulfinate ester 6.





**Figure 5.** M06-2X/6-31+G(d,p) computed rotational energy profiles of dimethyldisulfane **5** (left) and peroxythiosulfinate ester **6** (right). Conformers C–S–S–C are related by rotation about the torsion angle  $\theta$  in a counterclockwise movement about the C1–S1 bond relative to the S2–C2 bond. In **6**, the inner oxygen atom is red and the outer oxygen atom is a magenta color.



 $\theta = 41.5^{\circ}$   $\theta = 41.5^{\circ}$ 593

**6a** 59.5, 1.6

**6e** 129.5, 11.4 **6i** 179.5, 0 **6m** 229.5, 13.9 **6q** 289.5, 10 **6u** 339.5, 14.4

 $\theta = 102.3^{\circ}$ 

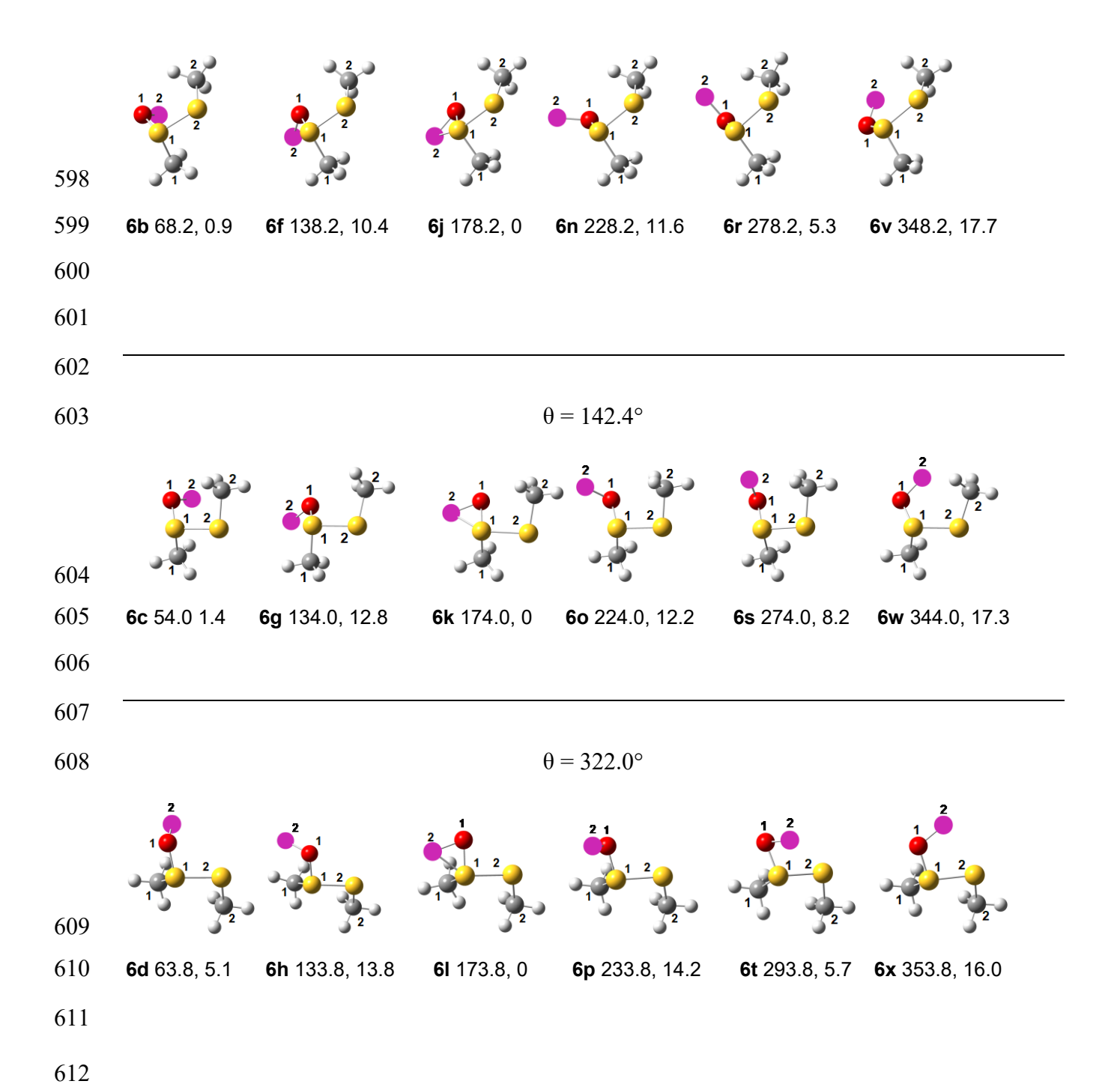
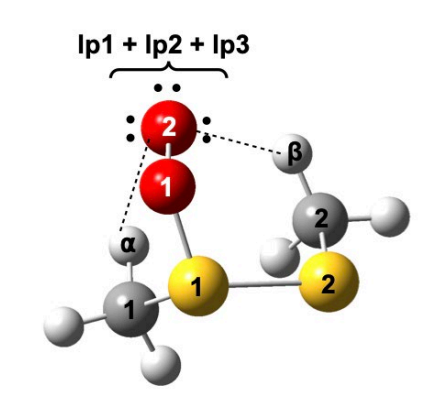


**Figure 6.** Three-dimensional computed energy plot for the 360° rotation about the dihedral angles  $\theta$  (C1–S1–S2–C2) and  $\phi$  (S2–S1–O1–O2). The torsional angles  $\theta$  (C1–S1–S2–C2) and  $\phi$  (S2–S1–O1–O2) were followed in 10° constrained increments each for the 360° rotation in a 36 × 36 grid. Conformers of C1–S1–S2–C2 are related by rotation about the torsion angle  $\theta$  in a

counterclockwise movement about the C1–S1 bond relative to the S2–C2 bond. Conformers of S2–S1–O1–O2 are related by rotation about the torsion angle  $\varphi$  in a counterclockwise movement about the S1–S2 bond relative to the O1–O2 bond. Values shown are  $\varphi$  (°) and  $\Delta E$  (kcal/mol).



625 <u>Donor Acceptor</u> <u>E (kcal/mol)</u>

 $O2_{lp} \rightarrow \sigma^*_{H\alpha\text{-C1}} \quad = \quad \text{-4.1}$ 

 $O2_{lp} \rightarrow \sigma^*_{H\beta-C2} = -3.5$ 

**Figure 7.** A Natural Bond Orbital (NBO) analysis of the outer oxygen atom lone pair electrons with the  $\sigma^*$  antibonding orbitals of H–C groups in peroxythiosulfinate ester **6**.